Journal of Geophysical Research: Solid Earth

Supporting Information for

Water Incorporation Mechanisms and Effects in $MgSiO_3$-majorite Under High Temperature and Pressure Conditions

Yancheng Lou[1,2,3,*], Zhigang Zhang[3,4], Andrew M. Walker[5], Stephen Stackhouse[6], Meng Chen[1,2], and Hongping He[1,2,4]

[1]State Key Laboratory of Deep Earth Processes and Resources, Guangzhou Institute of Geochemistry, Chinese Academy of Sciences, Guangzhou, 510640, China.
[2] Guangdong Research Center for Strategic Metals and Green Utilization, Guangzhou, 510640, China.
[3]Key Laboratory of Planetary Science and Frontier Technology, Institute of Geology and Geophysics, Chinese Academy of Sciences, Beijing 100029, China.
[4]College of Earth and Planetary Sciences, University of Chinese Academy of Sciences, Beijing 100049, China.
[5]Department of Earth Sciences, University of Oxford, South Park Road, Oxford OX1 3AN, United Kingdom.
[6]School of Earth and Environment, University of Leeds, Leeds LS2 9JT, United Kingdom.

Contents of this file

Text S1. Supplementary Methods

S1.1 estimation of the uncertainties of energy and relative ratio

The estimation method of uncertainties of energy is blocking method. We divide each equilibrated MD trajectory into five groups, each group involves 1800 steps and is larger than twice of common correlation time of MD simulations (Newman & Barkema, 1999). The uncertainties, therefore, are calculated by averaging standard deviation of groups. The uncertainties of the relative ratio are estimated by adjusting the free energies of mineral phases in R1-R14 (R8-14 are listed in Section S1.3) within standard deviations (SD) to obtain upper and lower limits. For example, the upper limit of the relative ratio of Mg1 hydrous Mgmj is estimated by selecting the case when the free energy of Mg1 hydrous Mgmj is the smallest (minus SD) and the others are the largest (plus SD), and the lower limit is obtained in the opposite case, i.e., the free energy of Mg1 hydrous Mgmj is the largest and the others are the smallest.

S1.2 several points need to be noted in the approach of this article

(1) Simulation size considerations and calculation of $H^*_{\text{hydrous Mgmj}}$. Due to current computational constraints, for Mgmj, usually only one unit cell (160 atoms) is used for AIMD simulations which leads to a water concentration of at least ~5600 or 11300 ppm (one Mg or Si hydrous defect). However, the solubility of water in Mgmj is generally ~700 ppm (Bolfan-Casanova et al., 2000; Katayama et al., 2003; Pigott et al., 2015), the upper limit may be only ~2700 ppm, depending on the synthesis experiment of a previous study (Thomas et al., 2015). Fortunately, this problem can be solved this way: firstly, the calculation of $\Delta_r G$ for the seven reactions can be described in another form (take R1 as an example):

$$\sum v_i \mu_i^* = \left(\mu^*_{\mathrm{Mg}_{32N-2}\mathrm{Si}_{32N}\mathrm{O}_{96N}\mathrm{H}_4(\mathrm{Mg1})} + 2\mu^*_{\mathrm{MgO}}\right) - \left(\mu^*_{\mathrm{Mg}_{32N}\mathrm{Si}_{32N-1}\mathrm{O}_{96N}\mathrm{H}_4(\mathrm{Si1})} + \mu^*_{\mathrm{SiO2}}\right) \quad (1)$$

where μ_i^* is chemical potential of pure phase $\underline{i}$. Based on the negligibility of vibrational entropy as mentioned in Section 2.1 in the main text. This can be rewritten as:

$$\begin{aligned}\sum v_i \mu_i^* = &\left[\left(H^*_{\mathrm{Mg}_{32N-2}\mathrm{Si}_{32N}\mathrm{O}_{96N}\mathrm{H}_4(\mathrm{Mg1})} - TS^*_{\mathrm{Mg}_{32N-2}\mathrm{Si}_{32N}\mathrm{O}_{96N}\mathrm{H}_4(\mathrm{Mg1}),\mathrm{conf.}}\right) + 2H^*_{\mathrm{MgO}}\right] \\ &- \left[\left(H^*_{\mathrm{Mg}_{32N}\mathrm{Si}_{32N-1}\mathrm{O}_{96N}\mathrm{H}_4(\mathrm{Si1})} - TS^*_{\mathrm{Mg}_{32N}\mathrm{Si}_{32N-1}\mathrm{O}_{96N}\mathrm{H}_4(\mathrm{Si1}),\mathrm{conf.}}\right) + H^*_{\mathrm{SiO2}}\right] \quad (2)\end{aligned}$$

where H_i^* and $S^*_{i,\mathrm{conf.}}$ represent the enthalpy and configurational entropy of pure phase $\underline{i}$, respectively. We now introduce $-NH^*_{\mathrm{Mgmj}}$ to both terms in square brackets, where H^*_{Mgmj} is the enthalpy of Mgmj per unit cell ($\mathrm{Mg}_{32}\mathrm{Si}_{32}\mathrm{O}_{96}$), N has the same meaning as in R1-7, e.g., for the hydrous Mgmj with a water concentration of ~1130 ppm, corresponding to the case where two Mg or one Si hydrous defect is present in a supercell comprising ten Mgmj unit cells (forming a system of 1602/1603 atoms), N equals 10. Equation (2) then becomes:

$$\sum v_i\mu_i^* = \left[\left(H^*_{\mathrm{Mg}_{32N-2}\mathrm{Si}_{32N}\mathrm{O}_{96N}\mathrm{H}_4(\mathrm{Mg1})} - TS^*_{\mathrm{Mg}_{32N-2}\mathrm{Si}_{32N}\mathrm{O}_{96N}\mathrm{H}_4(\mathrm{Mg1}),\mathrm{conf.}}\right) - NH^*_{\mathrm{Mgmj}} + 2H^*_{\mathrm{MgO}}\right] - \left[\left(H^*_{\mathrm{Mg}_{32N}\mathrm{Si}_{32N-1}\mathrm{O}_{96N}\mathrm{H}_4(\mathrm{Si1})} - TS^*_{\mathrm{Mg}_{32N}\mathrm{Si}_{32N-1}\mathrm{O}_{96N}\mathrm{H}_4(\mathrm{Si1}),\mathrm{conf.}}\right) - NH^*_{\mathrm{Mgmj}} + H^*_{\mathrm{SiO2}}\right] \quad (3)$$

we define the hydration enthalpy $\Delta H_{i,\mathrm{hydration}} = H^*_{i(\text{hydrous Mgmj with one hydrous defect})} - NH^*_{\mathrm{Mgmj}}$, which represents the enthalpy difference between dry and hydrous Mgmj arising from one hydrous defect. The $\Delta H_{i,\mathrm{hydration}}$ would not change even if there are a few hydrous defects of the same type in a unit cell as indicated by tests of Muir and Brodholt (2018). Hence, in this study, we considered the $\Delta H_{i,\mathrm{hydration}}$ for each type of hydrous defects in Mgmj to be identical at low water concentrations (less than ~1.13 wt.% which corresponds to the case of two Mg hydrous defects or one Si hydrous defect in a Mgmj unit cell). We calculate the hydration enthalpy for the Mg and Si hydrous defects separately using the following two equations:

$$\Delta H^*_{\text{Mg hydrous defect,hydration}} = H^*_{\mathrm{Mg}_{31}\mathrm{Si}_{32}\mathrm{O}_{96}\mathrm{H}_2(\text{one Mg hydrous defect})} - H^*_{\mathrm{Mgmj}} \quad (4)$$

$$\Delta H^*_{\text{Si hydrous defect,hydration}} = H^*_{\mathrm{Mg}_{32}\mathrm{Si}_{31}\mathrm{O}_{96}\mathrm{H}_4(\text{one Si hydrous defect})} - H^*_{\mathrm{Mgmj}} \quad (5)$$

and this means $H^*_{i(\text{hydrous Mgmj with } n \text{ hydrous defect})} = n * \Delta H_{i,\mathrm{hydration}} + NH^*_{\mathrm{Mgmj}}$ (in this study, $n = 1$ and 2 for Si and Mg hydrous defect, respectively). Based on this, the equation (3) can be expressed as:

$$\sum v_i\mu_i^* = \left[\left(2\Delta H_{\mathrm{Mg1,hydration}} - TS^*_{\mathrm{Mg}_{32N-2}\mathrm{Si}_{32N}\mathrm{O}_{96N}\mathrm{H}_4(\mathrm{Mg1}),\mathrm{conf.}}\right) + 2H^*_{\mathrm{MgO}}\right] - \left[\left(\Delta H_{\mathrm{Si1,hydration}} - TS^*_{\mathrm{Mg}_{32N}\mathrm{Si}_{32N-1}\mathrm{O}_{96N}\mathrm{H}_4(\mathrm{Si1}),\mathrm{conf.}}\right) + H^*_{\mathrm{SiO2}}\right] \quad (6)$$

where the subscripts of Mg1 and Si1 in $\Delta H_{i,\mathrm{hydration}}$ represent the type of hydrous defect causing the enthalpy difference. Notably, calculating the $S^*_{\mathrm{Mg}_{32N-2}\mathrm{Si}_{32N}\mathrm{O}_{96N}\mathrm{H}_4(\mathrm{Mg1}),\mathrm{conf.}}$ requires considering the situation of two Mg1 defects within a hydrous Mgmj unit cell (i.e., $\mathrm{Mg}_{32N}\mathrm{Si}_{32N-1}\mathrm{O}_{96N}\mathrm{H}_4$).

(2) The solution for unequal pressures of phases in each reaction in NVT simulations. Due to the differences among structures of seven kinds of hydrous Mgmj, the final pressures obtained by AIMD within the NVT ensemble are usually not identical and not exactly the target pressure p_0 but $p = p_0 + \delta p$. The common solution is to calculate the $F(V_0)$ curve which is obtained by fitting *F* as a function of volume at constant temperature, where V_0 is the volume corresponding to P_0. It is suitable for small systems, such as MgO and SiO_2 phases, but not suitable for phases of dry and hydrous Mgmj because of the higher computational costs caused by their large systems. Fortunately, Sun et al. (2018) report an approximation which defines $G^{\sim} = F(V) + p_0V$, and verified $G^{\sim}$ is very close to $G(p_0)$. The process is:

$$G^{\sim} = F(V) + p_0V$$
$$= F(V_0 + \delta V) + p_0(V_0 + \delta V)$$

$$= F(V_0) + (\frac{\partial F}{\partial V})_{V0}\delta V + p_0V_0 + p_0\delta V + \mathcal{O}(\delta V^2)$$
$$= G(p_0) + \mathcal{O}(\delta V^2) \ (7)$$

where $G(p_0) = F(V_0) + p_0V_0$; $\mathcal{O}(\delta V^2)$ is the higher order term which equals to $\frac{1}{2}(\partial^2 F/\partial V^2)_{V0}\delta V^2 = -\frac{1}{2}(\delta P^2 V_0/K_0)$, and K_0 is the bulk modulus at V_0. For example, K_0 is ~146.9 GPa and V_0 is ~9.8 Å^3/atom for Mgmj at 0 K and 0 GPa, even for $\delta p = 1$ GPa, $\mathcal{O}(\delta V^2)$ is only equal to ~0.208 meV/atom and can be ignored. In this study, the δp of dry and seven kinds of hydrous Mgmj were ~0.5 GPa (Table S1) which led to a smaller energy deviation and so was ignored.

(3) The ratio of seven kinds of hydrous Mgmj cannot be directly calculated at 0 K because the *T* cannot be zero in the equation of solving the equilibrium constant, i.e., $K = e^{-(\frac{\triangle G^{\Theta}_{p,T}}{RT})}$. However, the results could still be obtained by extrapolation. As shown in Fig. S2, the proportions of the seven kinds of hydrous defects are almost identical when we used static enthalpy plus the contribution of entropy treated by various temperatures (up to 300 K), i.e., $H^*_{i,\text{static}} + T_{(\text{up to } 300\text{ K})}S^*_{i,\text{config.}}$.

S1.3 calculation of elastic properties of Mgmj at static condition

Starting from the geometry produced by static energy minimization, 6 strain patterns, involving 3 axial (along each crystallographic axis) and 3 triclinic (shear strains), were applied and the resulting stresses calculated. The magnitudes of these strains were ± 0.1% and ± 0.3%. Then, adiabatic elastic constants (C^S_{ijkl}), which is equal to isothermal elastic constants at static conditions, were calculated by fitting a second-order polynomial to the strain-stress data (Table S4). The bulk and shear moduli (*K* and *G*) were calculated by Voigt-Reuss-Hill averages derived from the elastic constants (Anderson, 1963). Finally, the seismic wave velocities (v_p and v_s) were calculated from the formulas: $v_P = \sqrt{\frac{3K+4G}{3\rho}}$; $v_S = \sqrt{\frac{G}{\rho}}$.

Text S2. Supplementary Calculations

S2.1 another set of reactions which do not contain SiO_2

In previous works, the water incorporation mechanisms seemed to be affected by the activity of SiO_2 (Lemaire et al., 2004; Matveev et al., 2001). Therefore, we also used another set of reactions that do not contain SiO_2:

$$\mathrm{R8:\ Mg_{32N}Si_{32N-1}O_{96N}H_4(Si1) + Mg_2SiO_4 = Mg_{32N-2}Si_{32N}O_{96N}H_4(Mg1) + 4MgO}$$
$$\mathrm{R9:\ Mg_{32N}Si_{32N-1}O_{96N}H_4(Si2) + Mg_2SiO_4 = Mg_{32N-2}Si_{32N}O_{96N}H_4(Mg2) + 4MgO}$$
$$\mathrm{R10:\ Mg_{32N}Si_{32N-1}O_{96N}H_4(Si1) + Mg_2SiO_4 = Mg_{32N-2}Si_{32N}O_{96N}H_4(Mg3) + 4MgO}$$
$$\mathrm{R11:\ Mg_{32N-2}Si_{32N}O_{96N}H_4(Mg2) + 4MgO = Mg_{32N}Si_{32N-1}O_{96N}H_4(Si1) + Mg_2SiO_4}$$
$$\mathrm{R12:\ Mg_{32N-2}Si_{32N}O_{96N}H_4(Mg3) + 4MgO = Mg_{32N}Si_{32N-1}O_{96N}H_4(Si2) + Mg_2SiO_4}$$
$$\mathrm{R13:\ Mg_{32N-2}Si_{32N}O_{96N}H_4(Mg3) + 4MgO = Mg_{32N}Si_{32N-1}O_{96N}H_4(Si3) + Mg_2SiO_4}$$
$$\mathrm{R14:\ Mg_{32N-2}Si_{32N}O_{96N}H_4(Mg3) + 4MgO = Mg_{32N}Si_{32N-1}O_{96N}H_4(Si4) + Mg_2SiO_4}$$

The phase $\mathrm{Mg_2SiO_4}$ is forsterite at 0 K and 0, 10 GPa but ringwoodite at 0 K and 20 GPa as well as at 2000 K and ~20 GPa based on their phase stability fields (Yu et al., 2008). The settings of time-step and simulation time in first-principles molecular dynamics of ringwoodite are 10 ps and 1 fs, respectively. The results of the ratios of seven kinds of hydrous defects are shown in Fig. S3.

S2.2 the estimation of the effect of binding preference of H in Mg1 defect

The binding preferences of H in hydrous defects are observed in high-temperature simulations (Fig. S4), even when changing the initial configurations and increasing the simulation durations (Fig. S3). The calculation of $S^*_{i,\mathrm{conf.}}$ assumes no binding preferences between H^+ and O^{2-} in hydrous defect with unsaturated pairing, i.e., Mg1, Mg2, Mg3, and Si4 hydrous defects, because the probability of hydrogen connecting to oxygen is regarded as equal. Hence, the binding preferences of H will affect our results because of enthalpy differences caused by different defect configurations and deviations in $S^*_{i,\mathrm{conf.}}$. We evaluated the impact of these two issues separately**.** We chose hydrous Mgmj with the Mg1 hydrous defect in different configurations, because the $S^*_{i,\mathrm{conf.}}$ of the Mg1 hydrous defect is the largest (Table 2).

The first test showed that differences in energy between two Mg1 hydrous Mgmj are within 1.0 meV/atom and can be negligible (Table S2). Secondly, we tested the impact of preferred motions of H^+ on our results by comparing relative proportions of Mg1 hydrous Mgmj species calculated using $S^*_{i,\mathrm{conf.}}$ with and without considering binding preferences of H^+. We assumed that the configurations of binding between H and O in the Mg1 hydrous defect considering binding preferences is about $21^2/C_8^{2^2} = 0.563$ times that of not considering binding preferences, where $C_8^{2^2}$ is $(C_{NH+NE}^{NH})^{NV}$ (see Section 2.1 for details) for the Mg1 hydrous Mgmj, and a value of 21 is estimated by the trajectory of H^+ shown in Fig. S5 which indicated the number of combinations of two H^+ is about $4 \times 6 - 3 = 21$, $3 \times 7 - 3 = 19$, $5 \times 5 - 3 = 22$ for those shown in Fig. S5a, b, and c, respectively (considering only the number of O^{2-} that a single H^+ is most likely to bind to and subtracting the repeated and impossible configurations, i.e., two H^+ are bound to a same O^{2-}). Therefore, the proportion of the Mg1 hydrous Mgmj at 2000 K, 20 GPa, and 88 ppm,

which is the condition corresponding to the largest proportion of the Mg1 hydrous Mgmj in our results, will drop from ~6.8% to 3.9% when binding preferences of H^+ are considered. This case can be regarded as the lower limit because the binding preferences of H^+ in Mg2, Mg3, and Si4 hydrous defects are not considered simultaneously. However, this test demonstrates that accounting for binding preferences leads to a decrease in the proportion.

S2.3 the estimation of the effect of configurational entropy of mixed Mg hydrous defects

Since the number of Mg hydrous defects in hydrous Mgmj phase with Mg hydrous defects in R1-14 is greater than one, combinations of different types of Mg hydrous defect (Mg1, Mg2, Mg3) may yield results different from ours, which were derived from energy calculations of hydrous Mgmj phases containing only one single type of Mg hydrous defect. Therefore, we calculated the configurational entropy for systems with mixed Mg hydrous defects using the ratios of three Mg hydrous defects at water concentration of ~88 ppm conditions (i.e., about 790:156:1 for Mg1:Mg2:Mg3, as shown in Table S3). This condition corresponds to the largest ratio of Mg1 hydrous Mgmj in our results. The $S^*_{i,\mathrm{conf.}}$ for the hydrous Mgmj with mixed Mg defects can be described as:

$$S^*_{i,\mathrm{conf.}} = \sum k_B \ln\left[C^{NV_i}_{NV_i+NC_i}\left(C^{NH_i}_{NH_i+NE_i}\right)^{NV_i}\right]$$

The meaning of *NV*, *NC*, *NH*, and *NE* are explained in Section 2.1, the subscript *i* represent corresponding hydrous Mgmj defects in Mgmj, i.e., Mg1, Mg2, and Mg3 here. Like Eqn. (5), the $S^*_{i,\mathrm{conf.}}$ for one unit cell can be estimated by:

$$S^*_{i,\mathrm{conf.}} = \sum\left\{k_B[(nv_i + nc_i)\ln(nv_i + nc_i)] - nv_i\ln(nv_i) - nc_i\ln(nc_i)] + k_B\ln\left(C^{NH_i}_{NH_i+NE_i}\right)^{nv_i}\right\}$$
$$= \sum\left\{k_B[(x_i nv + nc_i)\ln(x_i nv + nc_i)] - x_i nv\ln(x_i nv) - nc_i\ln(nc_i)] + k_B\ln\left(C^{NH_i}_{NH_i+NE_i}\right)^{nv_i}\right\}$$

Where $nv_i = x_i nv$, x_i represents the mole fraction of component i, nv represent the number of Mg defects (vacancies) in a unit cell of hydrous Mgmj phase with mixed Mg defects, nc_i, NH_i, and NE_i are independent. The results show that its proportion is larger than the sum of proportions of three types of hydrous Mgmj containing the same type of Mg hydrous defects (~12.3% and ~8.12% for them, respectively; Table S3). If we consider the binding preference of H, the proportion will be lower. Therefore, the configurational entropy of mixed Mg hydrous defects does not affect the dominance of Si2 and Si3 defects within general water concentration ranges (at least ≥ 100 ppm).

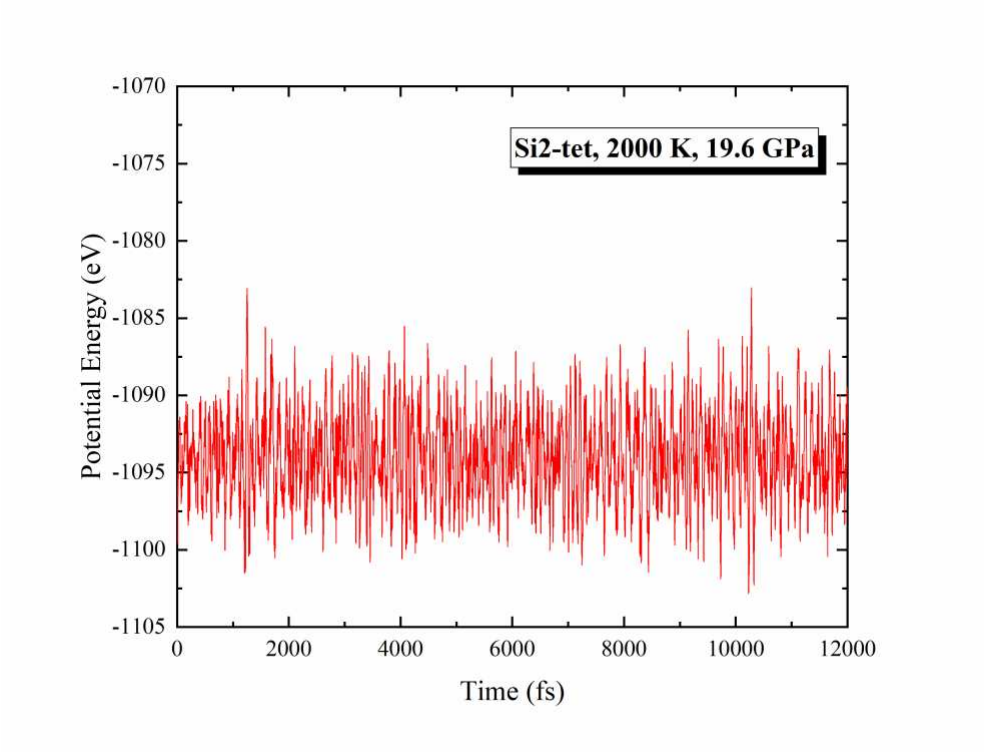

Figure S1. Fluctuations of the potential energy of hydrous Mgmj with Si2 hydrous defect in the equilibrium stage of a 2000 K molecular dynamics simulation.

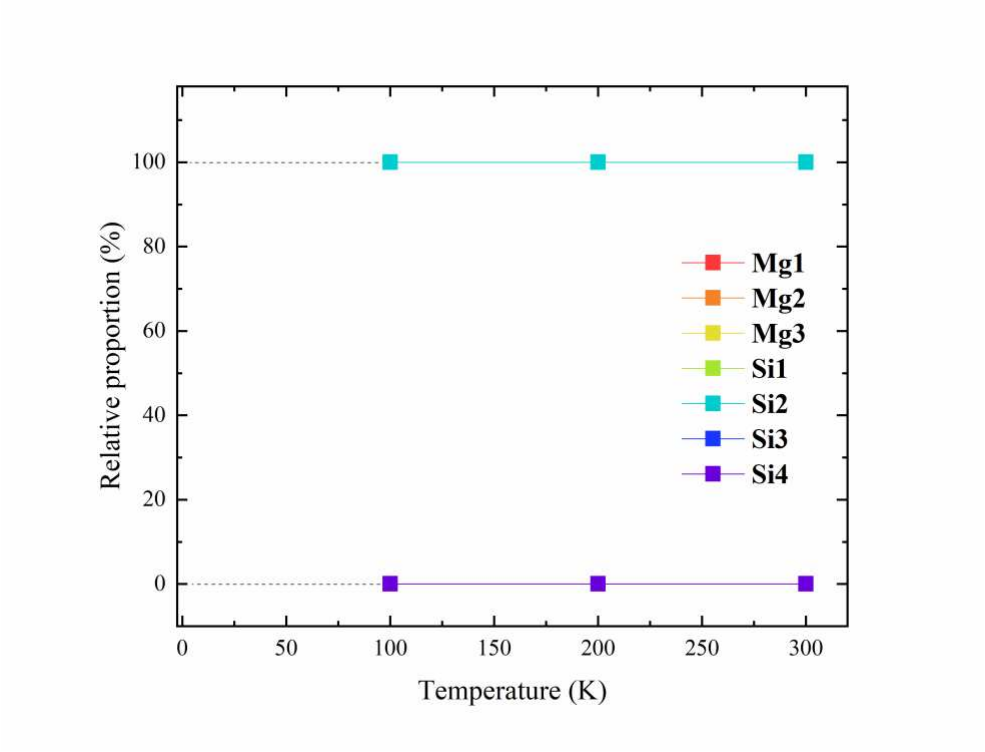

Figure S2. Extrapolation of relative proportion of seven kinds of hydrous defects in Mgmj to 0 K. Except for the values for the Si2 hydrous defect, the others are indistinguishable from the values of the Si4 hydrous defect.

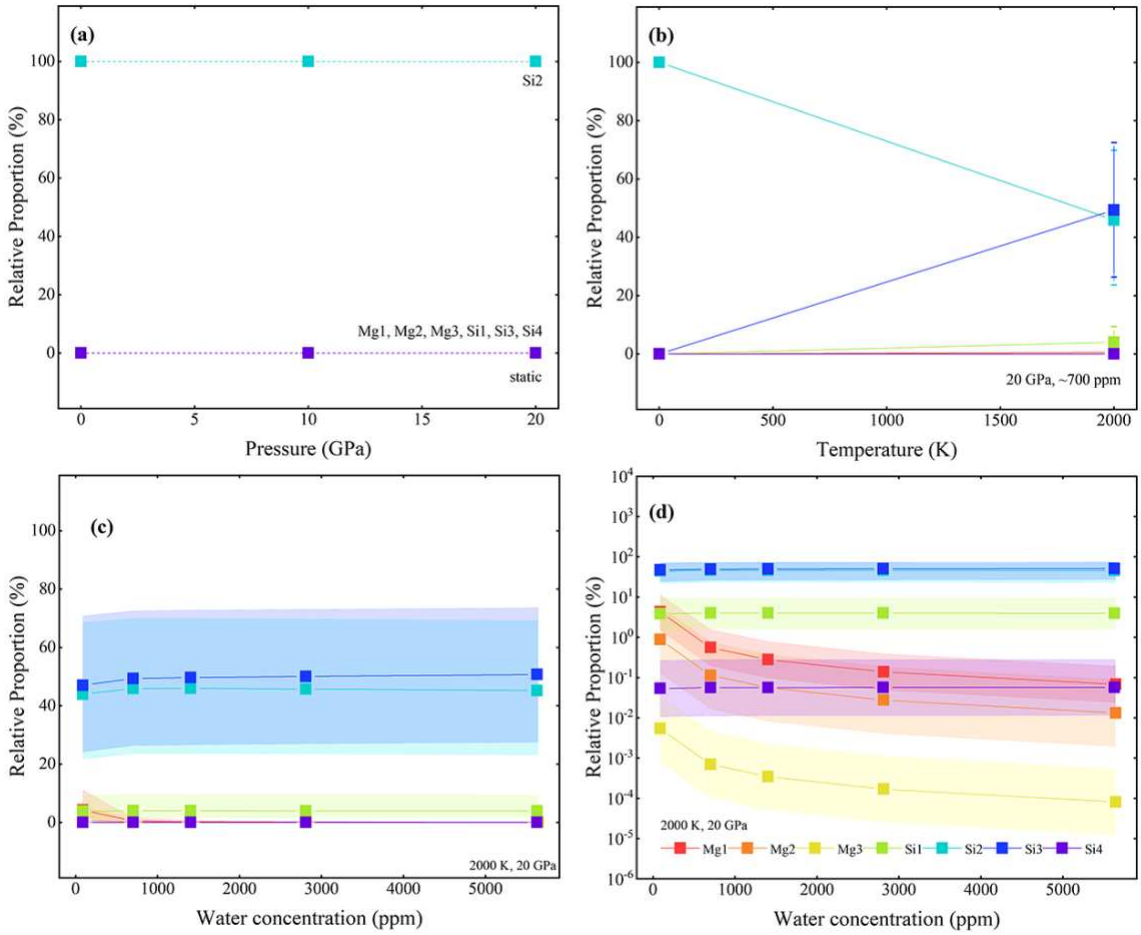

Figure S3. Relative proportions of seven kinds of hydrous Mgmj in sets of reactions which do not contain SiO_2 (R8-14). (a) shows the pressure dependence at 0 K, (b) shows temperature dependence at 20 GPa, and (c) and (d) show the dependence of water concentration at 2000 K and 20 GPa in linear and logarithmic terms, respectively. The straight lines connecting data points are guides to the eye. The confidence bands represent the estimated uncertainties in the values. Note that, except for the values for the Si2 and Si3 hydrous defects, the values for all other defects are in most cases indistinguishable from the values for the Si4 hydrous defect

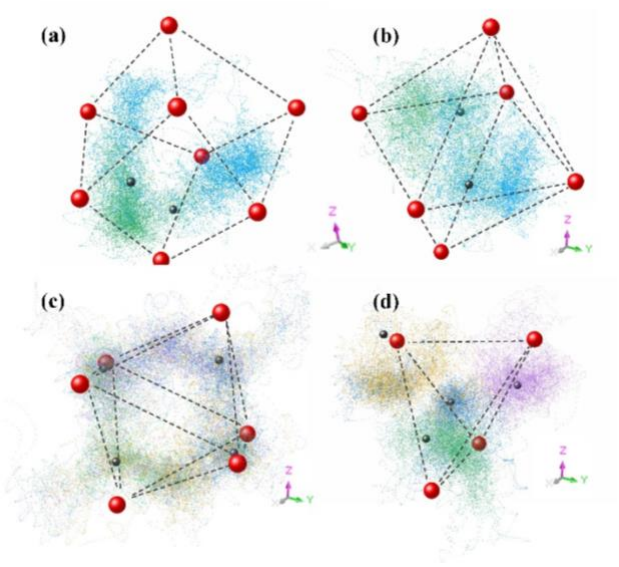

Figure S4. Example trajectories of H in (**a**) Mg1, (**b**) Mg3, (**c**) Si4, and (**d**) Si2 hydrous defects at 2000 K and ~20 GPa. Red and dark grey balls represent oxygens and hydrogens in the initial position, respectively. Dots of other colors represent the trajectories of hydrogens.

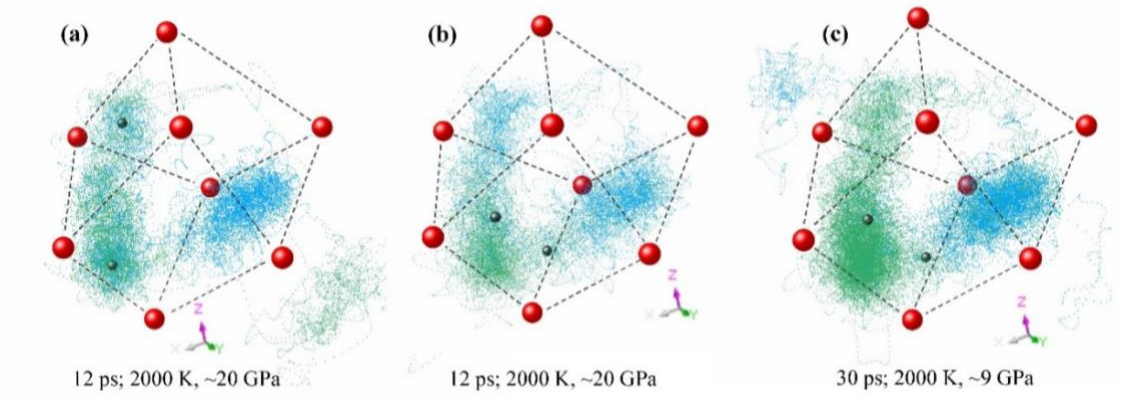

Figure S5. Movements of H in AIMD simulations of different initial configurations of Mg1 hydrous defect and simulation durations. Red and dark grey balls represent oxygens and hydrogens which are in the initial position, respectively. Dots of other colors represent the trajectories of hydrogen.

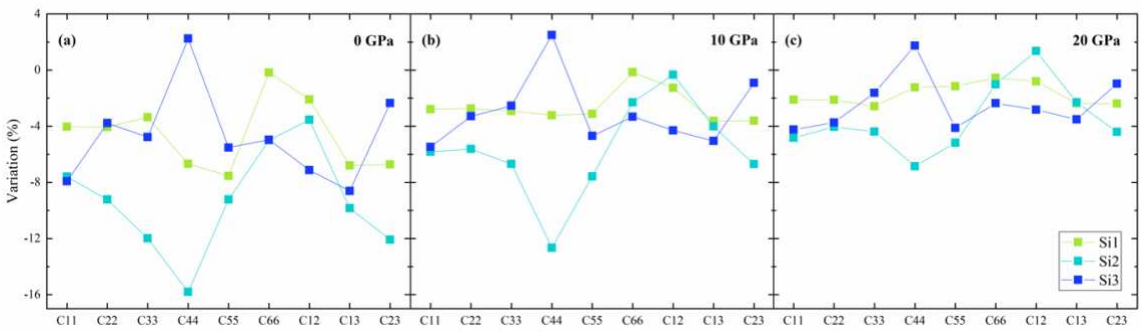

Figure S6. The variation of elastic constants caused by one Si1, Si2, and Si3 hydrous defect in Mgmj at 0 K.

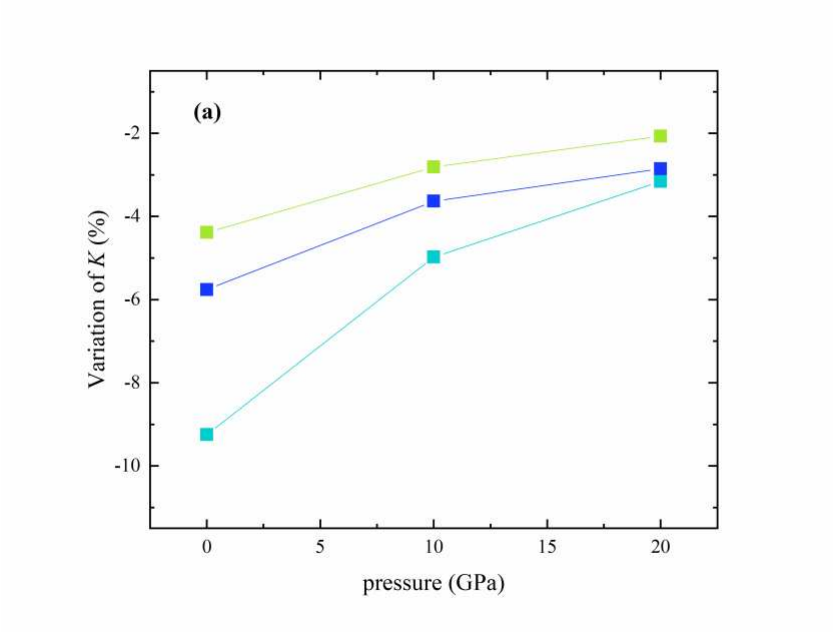

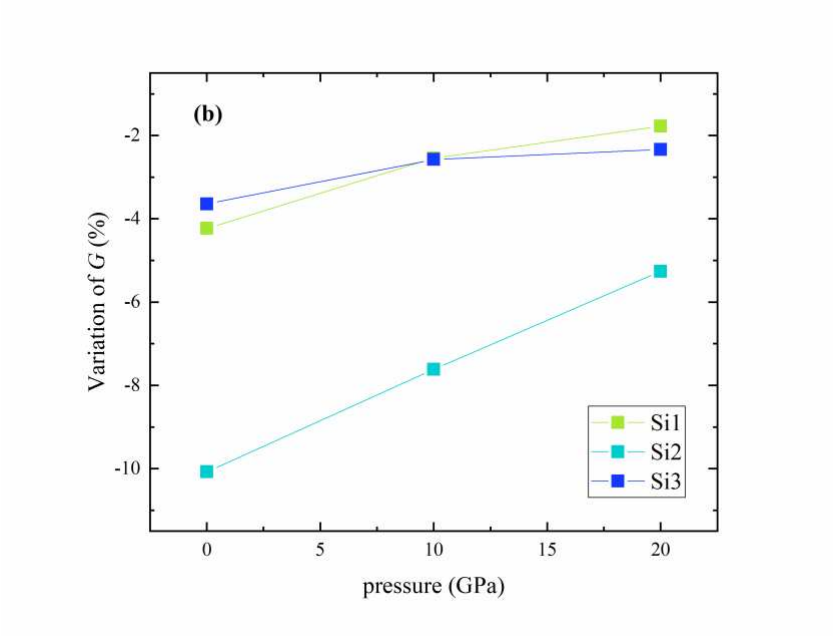

Figure S7. The variation of *K* and *G* caused by one Si1, Si2, and Si3 hydrous defect in Mgmj at 0 K.

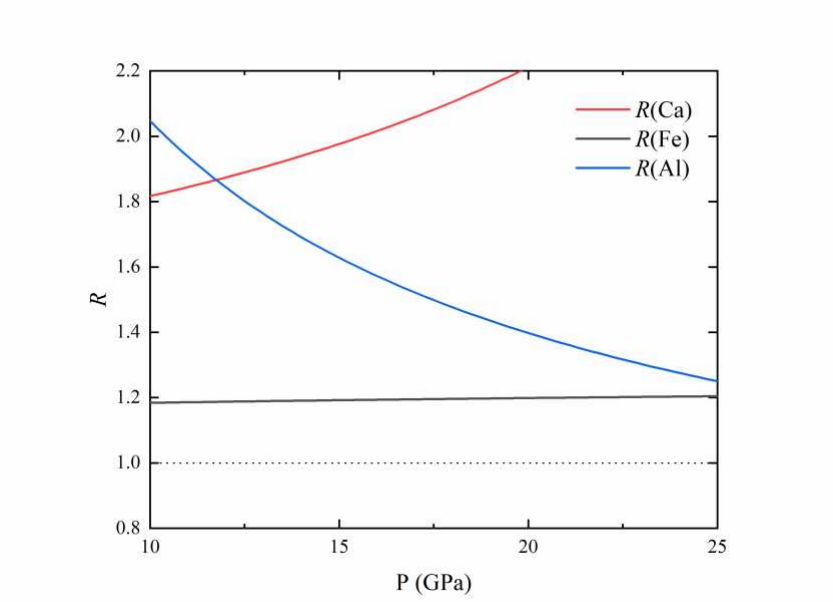

Figure S8. *R*(Ca), *R*(Fe), and *R*(Al) of garnet at ambient temperature as functions of pressure in a manner similar to *R*(H_2O): $\boldsymbol{R(Ca)} = \frac{\boldsymbol{\ln v_S(grossular) - \ln v_S(pyrope)}}{\boldsymbol{\ln v_P(grossular) - \ln v_P(pyrope)}}$, $\boldsymbol{R(Fe)} = \frac{\boldsymbol{\ln v_S(almandine) - \ln v_S(pyrope)}}{\boldsymbol{\ln v_P(almandine) - \ln v_P(pyrope)}}$, and $\boldsymbol{R(Al)} = \frac{\boldsymbol{\ln v_S(pyrope) - \ln v_S(Mgmj)}}{\boldsymbol{\ln v_P(pyrope) - \ln v_P(Mgmj)}}$. The elastic data are taken from: grossular (Gwanmesia et al., 2014; Kono et al., 2010), almandine (Arimoto et al., 2015),

Mgmj (Zhou et al., 2021), and pyrope (Chantel et al., 2016; Gwanmesia et al., 2006; Zou et al., 2012).

	conditions				
	0 K			2000 K	
Phase	V (Å^3, 0 GPa)	V (Å^3, 10 GPa)	V (Å^3, 20 GPa)	P (GPa)	V (Å^3)
Mgmj	1565.98	1475.67	1407.52	19.68	1475.67
Mg1	1568.62	1476.60	1407.50	19.62	1476.60
Mg2	1567.31	1474.41	1405.67	19.73	1474.41
Mg3	1567.63	1474.42	1405.01	19.61	1474.42
Si1	1572.54	1478.59	1408.66	19.79	1478.59
Si2	1579.42	1481.71	1410.62	19.62	1481.71
Si3	1576.62	1481.53	1411.00	19.52	1481.53
Si4	1582.52	1485.58	1412.09	19.49	1485.58
forsterite	75.00	69.72	-	-	-
ringwoodite	-	-	61.63	20.35	64.32
alpha-quartz	40.32	-	-	-	-
stishovite	-	23.31	22.63	20.00	*23.56
periclase	19.29	18.18	17.33	20.00	*18.42

Table S1. Volumes of dry and hydrous Mgmj, pyrope, α-quartz, stishovite, and periclase under different pressures in this study. Mg1-Si4 represents hydrous Mgmj with one corresponding hydrous defect, and the symbol * represents the data fitted from the 3rd-order Birch-Murnaghan EOS.

Time-step	U (eV) at 2000 K, ~9 GPa			
	1 fs	SD	0.5 fs	SD
Si2 (tet), total 12 ps	-1055.222	0.085	-1055.159	0.311
Initial binding of H^+	U (eV) at 2000 K, ~20 GPa			
	O3	SD	O4 and O5	SD
Mg1 (dod), total 12ps	-1049.217	0.266	-1049.252	0.046

Table S2. Comparisons of energies of hydrous Mgmj corresponding to one unit cell of dry Mgmj obtained from different settings of AIMD simulations. SD represents Standard deviation.

88 ppm	88 ppm

Mg1	0.066	Mg-mixed	0.123
Mg2	0.014	-	
Mg3	8.3E-05	-	
Si1	0.037	Si1	0.035
Si2	0.427	Si2	0.411
Si3	0.456	Si3	0.430
Si4	5.2E-04	Si4	5.0E-04

Table S3. Comparisons of proportions of hydrous Mgmj obtained from energy calculations between considering configurational entropy of single and mixed Mg hydrous defects at a water concentration of 88 ppm, 2000 K, and 20 GPa.

Type	*p*	C11	C12	C13	C14	C15	C16	C22	C23	C24	C25	C26	C33	C34	C35	C36	C44	C45	C46	C55	C56	C66
	0	254.17	96.60	86.75	0.70	-3.40	12.55	246.15	86.88	0.81	3.31	-17.35	229.68	2.03	0.84	-1.20	68.90	3.69	-1.24	66.51	1.56	79.42
Mg3	10	310.93	134.65	123.37	0.87	-5.40	21.11	303.19	123.38	1.97	1.72	-21.80	306.50	0.63	0.16	-0.75	80.51	1.52	-0.06	77.92	0.35	94.29
	20	362.26	169.76	158.84	0.46	-5.37	24.85	355.80	158.60	1.61	0.55	-24.43	368.54	-0.37	0.36	-0.81	90.34	0.39	0.19	88.49	-0.16	104.89
	0	251.43	99.89	83.73	0.01	0.01	13.66	251.38	83.79	0.02	-0.01	-13.67	229.86	0.05	-0.05	0.00	66.64	-0.01	0.00	66.02	0.00	85.12
Si1	10	307.99	135.11	120.72	0.01	0.06	20.75	308.16	120.74	-0.01	-0.08	-20.69	306.43	0.02	-0.01	0.01	80.16	-0.01	0.00	80.24	0.00	97.36
	20	359.25	169.81	156.51	0.01	-0.01	25.05	359.18	156.48	0.01	-0.02	-24.97	367.34	-0.01	-0.02	0.03	90.84	0.01	0.00	90.91	0.00	106.00
	0	242.10	98.41	81.00	-0.53	1.18	11.22	237.85	78.99	2.15	0.80	-7.89	209.33	2.18	-0.88	1.90	60.12	0.14	-0.61	64.82	-0.26	81.01
Si2	10	298.38	136.40	120.23	-2.36	1.46	18.89	299.02	116.87	1.02	0.54	-16.27	294.52	0.73	-2.61	1.47	72.34	1.35	-0.42	76.54	-1.73	95.27
	20	349.29	173.51	156.62	-2.50	1.57	22.53	352.13	153.24	0.89	0.49	-21.13	360.52	0.06	-2.62	0.60	85.66	0.86	0.04	87.20	-2.33	105.51
	0	241.25	94.75	82.10	0.77	0.77	9.12	252.10	87.73	-3.24	0.56	-10.42	226.50	0.70	3.39	2.47	73.01	0.44	0.05	67.46	1.38	81.04
Si3	10	299.49	130.97	118.94	1.13	1.13	16.36	306.39	124.12	-2.15	0.02	-17.53	307.60	0.70	4.16	0.05	84.89	-0.44	0.33	78.93	2.35	94.27
	20	351.43	166.36	154.67	1.64	1.34	20.51	353.27	158.76	-1.49	0.17	-21.59	370.96	0.74	3.78	-0.89	93.57	-1.22	0.77	88.18	2.80	104.08

Table S4. Elastic constants of hydrous Mgmj with Mg3, Si1, Si2, and Si3 hydrous defect at 0 K. The units for *p* (pressure) and C_{ij} are GPa.

References

Anderson, O. L. (1963). A simplified method for calculating the Debye temperature from elastic constants. *Journal of Physics and Chemistry of Solids*, *24*(7), 909–917.

Arimoto, T., Gréaux, S., Irifune, T., Zhou, C., & Higo, Y. (2015). Sound velocities of Fe3Al2Si3O12 almandine up to 19 GPa and 1700 K. *Physics of the Earth and Planetary Interiors*, *246*, 1–8. https://doi.org/10.1016/j.pepi.2015.06.004

Bolfan-Casanova, N., Keppler, H., & Rubie, D. C. (2000). Water partitioning between nominally anhydrous minerals in the MgO–SiO2–H2O system up to 24 GPa: Implications for the distribution of water in the Earth's mantle. *Earth and Planetary Science Letters*, *182*(3–4), 209–221.

Chantel, J., Manthilake, G. M., Frost, D. J., Beyer, C., Ballaran, T. B., Jing, Z., & Wang, Y. (2016). Elastic wave velocities in polycrystalline Mg_3 Al_2 Si_3 O_{12} -pyrope garnet to 24 GPa and 1300 K. *American Mineralogist*, *101*(4), 991–997. https://doi.org/10.2138/am-2016-5335

Gwanmesia, G. D., Wang, L., Heady, A., & Liebermann, R. C. (2014). Elasticity and sound velocities of polycrystalline grossular garnet (Ca3Al2Si3O12) at simultaneous high pressures and high temperatures. *Physics of the Earth and Planetary Interiors*, *228*, 80–87.

Gwanmesia, G. D., Zhang, J., Darling, K., Kung, J., Li, B., Wang, L., Neuville, D., & Liebermann, R. C. (2006). Elasticity of polycrystalline pyrope (Mg3Al2Si3O12) to 9 GPa and 1000 C. *Physics of the Earth and Planetary Interiors*, *155*(3–4), 179–190.

Katayama, I., Hirose, K., Yurimoto, H., & Nakashima, S. (2003). Water solubility in majoritic garnet in subducting oceanic crust. *Geophysical Research Letters*, *30*(22).

Kono, Y., Gréaux, S., Higo, Y., Ohfuji, H., & Irifune, T. (2010). Pressure and temperature dependences of elastic properties of grossular garnet up to 17 GPa and 1 650 K. *Journal of Earth Science*, *21*(5), 782–791. https://doi.org/10.1007/s12583-010-0112-2

Lemaire, C., Kohn, S. C., & Brooker, R. A. (2004). The effect of silica activity on the incorporation mechanisms of water in synthetic forsterite: A polarised infrared spectroscopic study. *Contributions to Mineralogy and Petrology*, *147*, 48–57.

Matveev, S., O'neill, H. S. C., Ballhaus, C., Taylor, W. R., & Green, D. H. (2001). Effect of silica activity on OH- IR spectra of olivine: Implications for low-a SiO2 mantle metasomatism. *Journal of Petrology*, *42*(4), 721–729.

Muir, J. M. R., & Brodholt, J. P. (2018). Water distribution in the lower mantle: Implications for hydrolytic weakening. *Earth and Planetary Science Letters*, *484*, 363–369. https://doi.org/10.1016/j.epsl.2017.11.051

Newman, M. E., & Barkema, G. T. (1999). *Monte Carlo methods in statistical physics*. Clarendon Press. https://books.google.com/books?hl=zh-CN&lr=&id=HgBREAAAQBAJ&oi=fnd&pg=PR9&dq=Monte+Carlo+Methods+in+Statistical+Physics&ots=rvsFcyokGA&sig=6Is8rZ2zC6uqlIDNIBLzyogc6EE

Pigott, J. S., Wright, K., Gale, J. D., & Panero, W. R. (2015). Calculation of the energetics of water incorporation in majorite garnet. *American Mineralogist*, *100*(5–6), 1065–1075.

Sun, T., Brodholt, J. P., Li, Y., & Vočadlo, L. (2018). Melting properties from ab initio free energy calculations: Iron at the Earth's inner-core boundary. *Physical Review B*, *98*(22), 224301.

Thomas, S.-M., Wilson, K., Koch-Müller, M., Hauri, E. H., McCammon, C., Jacobsen, S. D., Lazarz, J., Rhede, D., Ren, M., & Blair, N. (2015). Quantification of water in majoritic garnet. *American Mineralogist*, *100*(5–6), 1084–1092.

Yu, Y. G., Wu, Z., & Wentzcovitch, R. M. (2008). *α–β–γ* transformations in Mg2SiO4 in Earth's transition zone. *Earth and Planetary Science Letters*, *273*(1), 115–122. https://doi.org/10.1016/j.epsl.2008.06.023

Zhou, C., Gréaux, S., Liu, Z., Higo, Y., Arimoto, T., & Irifune, T. (2021). Sound Velocity of $MgSiO_3$ Majorite Garnet up to 18 GPa and 2000 K. *Geophysical Research Letters*, *48*(14), Article 14. https://doi.org/10.1029/2021GL093499

Zou, Y., Irifune, T., Gréaux, S., Whitaker, M. L., Shinmei, T., Ohfuji, H., Negishi, R., & Higo, Y. (2012). Elasticity and sound velocities of polycrystalline Mg3Al2 (SiO4) 3 garnet up to 20 GPa and 1700 K. *Journal of Applied Physics*, *112*(1). https://pubs.aip.org/aip/jap/article/112/1/014910/213590